View metadata, citation and similar papers at core.ac.uk
brought to you by CORE
provided by KHALSA PUBLICATIONS

ISSN 2347-3487

MAGNETIC AND ELECTRICAL PROPERTIES OF ELECTRON BEAM GUN DEPOSITED [Mn/Al] MULTILAYERED FILMS

R.Ramanna[a], T.Sankarappa[a]*, T. Sujatha[a], J.S. Ashwajeet[a] and P.J. Sadashivaiah[b]
[a]Department of Physics, Gulbarga University, Gulbarga, Karnataka, India
[b]Shridevi Institute of Engineering and technology, Tumkur, Karnataka, India
*Author for correspondence: sankarappa@rediffmail.com

ABSTRACT

By following electron beam gun evaporation technique, the magnetic multilayers in the configuration, $[Mn(60nm)/Al(20nm)]_n$; n =1, 2 and 9 were deposited at 473K, under high vacuum conditions. From grazing incidence X-ray diffraction (GIXRD) studies, the grain sizes were determined and they were in the order of few nanometers. Atomic force microscope (AFM) were employed to study surface structure and grain sizes. The magnetization as a function of field at 150K and 200K have been measured using the MPMS SQUID - vibrating sample magnetometer (VSM). From the hysteresis loops, coercive field, saturation magnetization, remanent magnetization and antiferromagnetic coupling were determined. All the three films hinted at the existence of at antiferromagnetic interaction between Mn layers through Al layer. Electrical resistivity in the temperature range from 5K to 300K has been measured. Films exhibited semiconducting to metallic transition. The power law variation of resistivity with temperature was established for the metallic region. Conductivity data for semiconducting region of a film has been analysed using polaran hopping models, activation energy and density of states at Fermi level were established. This is for the first time that antiferromagnetic coupling between Mn layers through interfacer layer and semiconducting to metallic transition have been noticed in the present configuration of [Mn/Al] multilayers.

Keywords

Multilayered films, GIXRD, Surface roughness, Coercive field, Resistivity.

ISSN 2347-3487

1. INTRODUCTION

Magnetic and electrical transport studies on magnetic multilayers have been of great interest in the recent years. Multilayers consisting of ferromagnetic metals and nonmagnetic metals were investigated for structure, magnetic and electrical studies [1-6]. The role of nonmagnetic spacer in tuning the interlayer exchange coupling (IEC) between two neighboring magnetic layers has been first reported by Grunberg [7.] Subsequently, giant magnetoresistance (GMR) and oscillations in IEC with varying width of the nonmagnetic spacer were discovered [8-10]. In some multilayers, chromium (Cr) spacer was used and investigated interface roughness [11, 12], magnetic and electronic structures [13]. An anomalous behavior of low temperature resistivity has been observed in the films, Co/M/Co (M = Cr or Cr/Ag or Ag/Cr) [14]. The effect of Cu interlayer on grain size was studied in sputtered Fe/Cu multilayers [15]. Structural and magnetic properties were probed in Fe/Cu multilayers for varied Fe layer thickness [16]. Interlayer diffusion of nonmagnetic metals C, Cr, Pt [17, 18], Ag [19], Al and Cu into the magnetic layers has been studied [20]. Some Mn-based alloys and compounds exhibited ferromagnetism though they did not contain ferromagnetic elements. The systems, Mn/Al [21], Mn/C/Si [22, 23] and Mn/SiO2/Si [24] showed ferromagnetism at room temperature. In these systems, it was learnt that Mn lattices become ferromagnetic and that the ferromagnetic regions were located near the Mn/Al interfaces [25]. It is known that the interlayer coupling depends on the thickness of spacer layer. Here we report on structural, magnetic and electrical properties of multilayered films, $[Mn(60nm)/Al(20nm)]_n$ (where n= 1,2,9 represent number of repeats) labeled as MAM1, MAM2 and MAM3. For the first time a detailed studies of structural, magnetic and low temperature electrical properties of [Mn/Al] multilayers are reported.

2. EXPERIMENTAL

The $[Mn/Al]_n$; n= 1, 2, 9 films were deposited in a diffusion pump evacuated coating unit using electron beam gun evaporation method at a temperature of 473K. X- ray diffraction (GIXRD) studies were carried out in Brucker-D8 advance diffractometer with Cu-Kα radiation of 1.5406 Å wavelength. Surface morphology has been investigated by Atomic force microscope (AFM). Average surface roughness of the films were determined on a scan area of 1 μm x 1 μm using Nanoscope software. Magnetic hysteresis studies were carried out in an MPMS SQUID – vibrating sample magnetometer (VSM). The resistivity measurements were done by following a four point method in the temperature range from 5 K to 300K in an Oxford Instrument make setup.

3. RESULTS AND DISCUSSION

3.1 Grazing incidence X-ray diffraction (GIXRD) studies:

The XRD spectra for 2θ between 20° and 60° for MAM1 film is shown in Fig. 1(a) and the Gaussian fit to the peak is depicted in Fig. 1(b). The spectra exhibit single sharp peak at around 43° and that could be due to a plane of Mn crystals indicating (411) reflection. This result is comparable with that reported for Mn-Al multilayers [21]. No other peaks are seen in the spectrum up to 60°. The average grain sizes have been estimated using Scherrer's formula [26], $D = (0.9\lambda)/(B \cos\theta_B)$, where D is the grain size, B the angular width in terms of 2θ, θ_B the Bragg angle and λ the wavelength of the radiation. The interplanar spacing of the films were calculated using the relation, $d = \lambda/(2 \sin\theta_B)$ [Table.1].

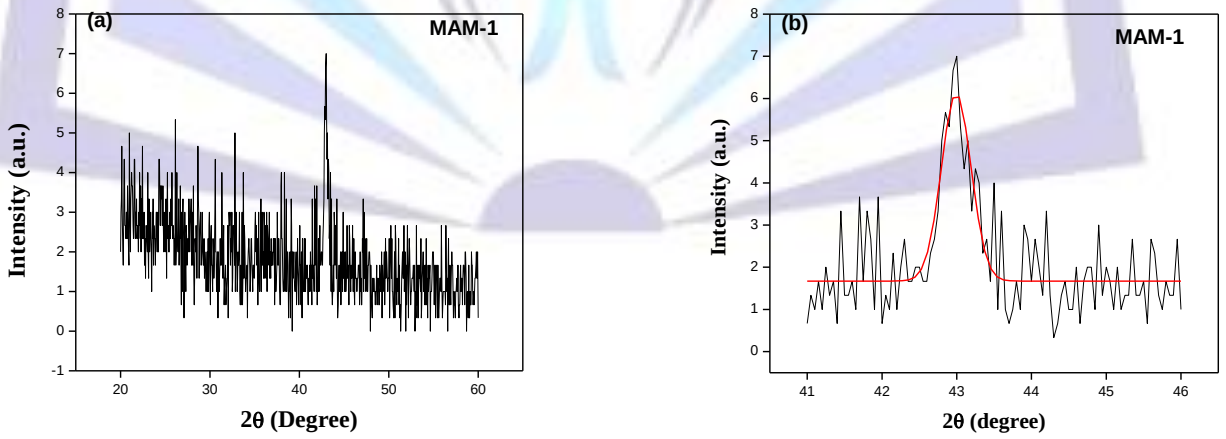

Fig.1: (a) GIXRD spectra for MAM1 film and (b) spectra around the peak position. The solid line is a Gaussian fit to the peak.

The average grain sizes obtained were of about 21nm and interplanar spacing of 2.1Å for all the three films. These observations show that the present films are nanocrystalline in nature [26]. Crystalline to quasicrystalline phase transition was observed at 873k in [Mn/Al] multilayers due to interfacial diffusion [27]. No such transition can be expected in the present films as the experiments are conducted much below 873k.

Table.1. Parameters extracted from the GIXRD spectra.

Film	Peak position (2θ)	Peak width (degrees)	Grain size, D (nm)	Interplanar spacing, d(Å)
MAM1	42.993	0.397	21.480	2.101
MAM2	43.026	0.375	21.729	2.100
MAM3	42.981	0.404	21.124	2.102

3.2 AFM

AFM images in contact mode with a scan area of 1 μm x 1 μm have been recorded. The AFM images in 2D and 3D for the present films are shown in Fig. 2. The height verses distance profiles were sketched [28]. This analysis provided information on average grain size, D (pair of blue dots) and average surface roughness, h [pair of green dots in Fig. (2a)] of the films. It can be seen that D and h increases with increase of t [Table 2]. Increase of grain sizes on the surface with increase of t is quite obvious on the 3D images Surface roughness also increased with increase in t.

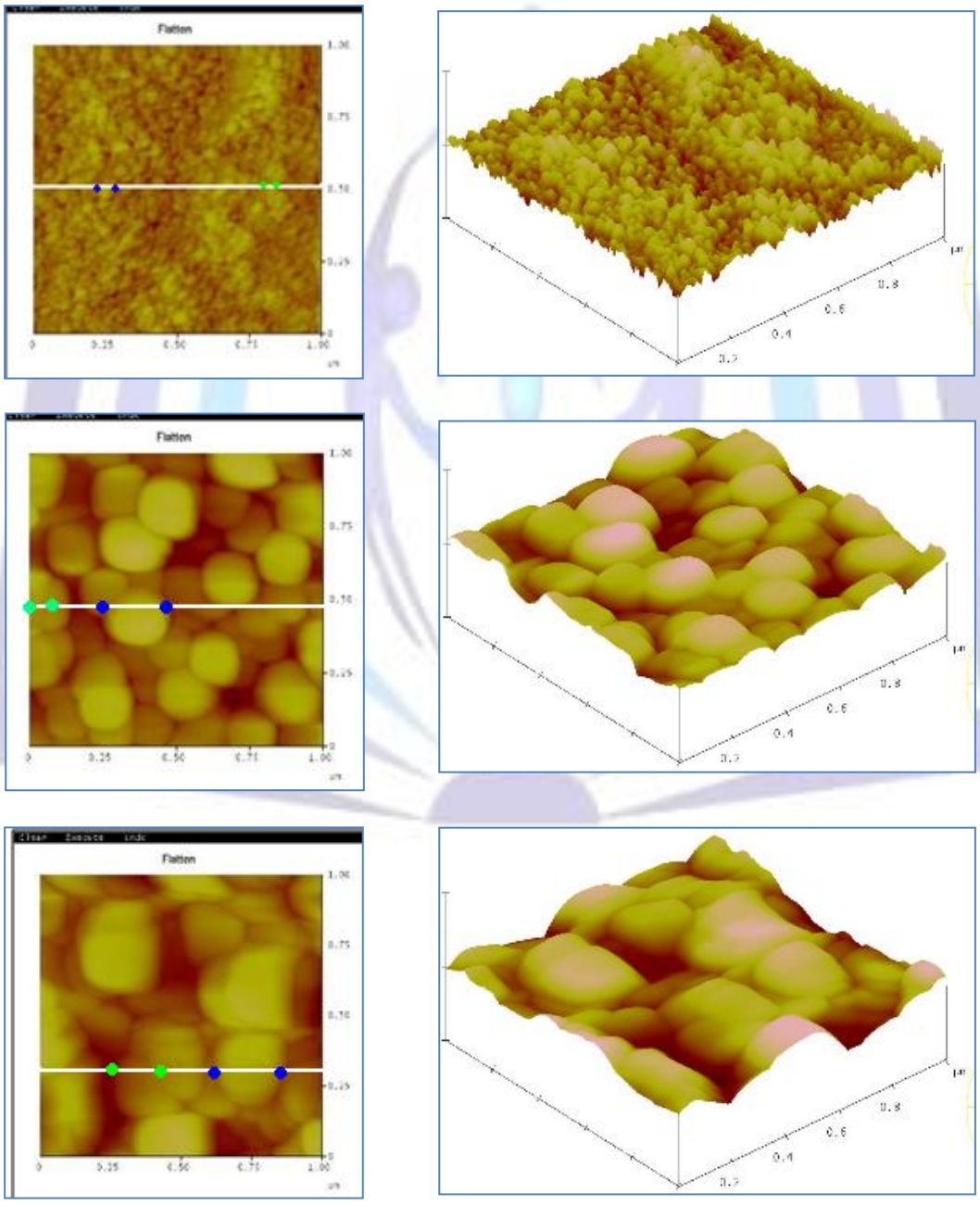

(a) **(b)**

Fig.2. AFM image of MAM1, MAM2 and MAM3 films in (a) 2D and (b) 3D

Table 2: AFM parameters of MAM sample.

Sample	Surface roughness, h (nm)	Average particle size, D (nm)
MAM1	2.13	101
MAM2	4.41	373
MAM3	22.22	477

The grain sizes obtained from XRD and AFM are quite different. It can be due to the fact that AFM images provide sizes of grains only on the surface only. Where as XRD gives information about average size of the grains in the entire bulk of the sample. Therefore, the grain sizes obtained by these two techniques are different.

3.3 Magnetization

The magnetization, M, as a function of applied field, H, was measured at two different temperatures of 150K and 200K for the fields applied parallel to the surface of the films. The recorded hysteresis (M-H) loops for the present films are shown in Fig.3. All the three films exhibited ferromagnetism at these two temperatures. Coercive field, H_c, saturation magnetization, M_s, remanent magnetization, M_r, were determined from the hysteresis loops and they are tabulated in Table.3. H_c is found to be increasing with increase of temperature for MAM1 film and it is decreasing as a function of temperature for MAM3. It means that film MAM1 become magnetically hardened with increasing temperature and MAM3 become softened with temperature.

Saturation magnetization M_s, remenant magnetization M_r and antiferromagnetic coupling decreased with increasing temperature in the present films [Table.3]. The size of the saturation magnetization measured in the present film is very small and that is expected for when the films are grown on the glass substrates [21]. The increase of saturation magnetization with decrease in temperature observed in these films agree with the results of other multilayers [29]. Total magnetization has been found to be dependent on the Mn/Al layer thickness [25]. In the present films Mn/Al layers thickness was kept constant and the number of repeats was varied. Due to non-availability of the instrument magnetization of MAM2 film could not be measured.

Table 3: Parameters derived from the M-H loops at 150K and 200K for MAM Samples.

Sample	Temperature, K	Coercive field, H_c (T) $x10^{-2}$	Saturation magnetization, M_s (Am^{-1}) $x10^{-2}$	Remanent magnetization, M_r (Am^{-1}) $X10^{-2}$	Squareness (M_r/M_s) S	AF coupling (1-S)
MAM1	150	0.704	1.636	0.212	0.129	0.870
	200	1.393	0.334	0.138	0.414	0.585
MAM3	150	1.801	1.781	0.557	0.313	0.686
	200	1.591	0.321	0.133	0.414	0.585

The finite values of (1-S) obtained for these films confirm the existence of antiferromagnetic type of interaction between Mn layers through similar to what has been observed in [26,30]. The strength of antiferromagnetic coupling decreases with increasing temperature [10].

ISSN 2347-3487

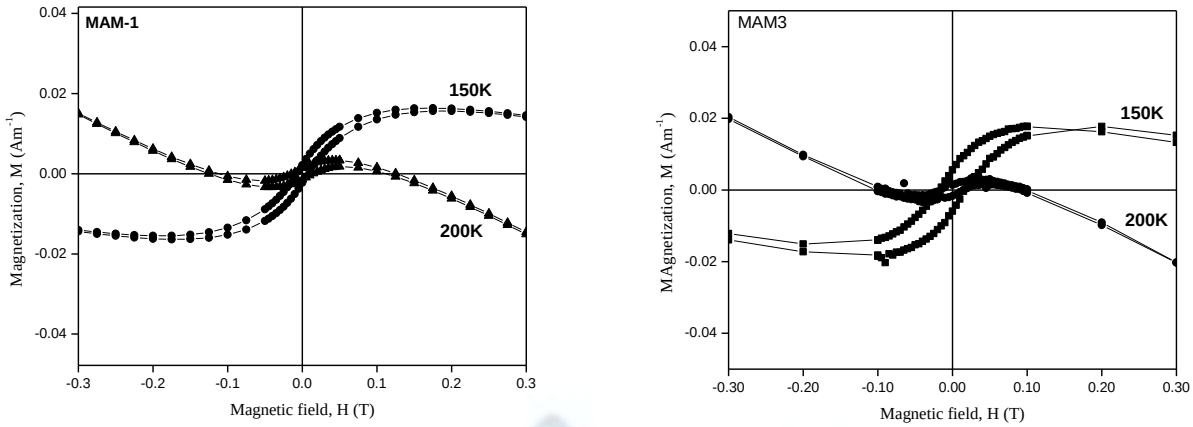

Fig.3. Plots of magnetization versus magnetic field for MAM1 and MAM3 films.

3.4 Resistivity Studies

The measured variations of ρ with T for all the three films are displayed in Fig. 4(a-c). All the three films exhibited semiconducting to metal transition (MST) [31]. The MST transition shown by the present films is similar to Ni/Al/Ni sandwich films and Zno doped systems [32, 33]. Transition temperature, T_c measured are recorded in Table. 4. Tc decreases with increasing number of repeats of bilayers in the films. This means that MAM1 has got longer tail in the semiconducting region than the metallic region. Where as other two films exhibited longer tails in the metallic region than the semiconducting region.

Table 4: Measured transition temperature (Tc), of the films.

Sample	MAM1	MAM2	MAM3
Tc (K)	167	45	6

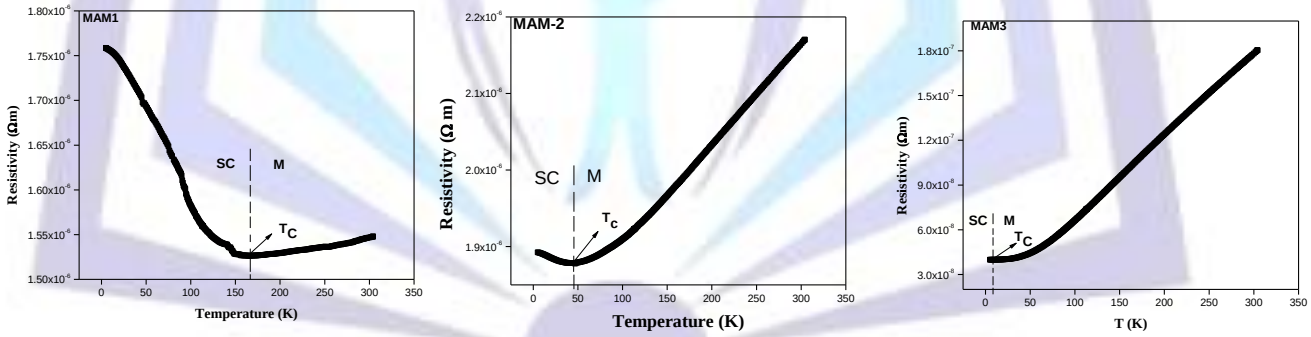

Fig. 4: A plot of resistivity, ρ, versus temperature, T, for MAM1, MAM2 and MAM3 films.

3.4.1 Resistivity variation in MAM1 film

The conductivity data of MAM1 film in the semiconducting region has been analysed using Mott's small polaron hopping and variable range hopping models due to Mott's and Greaves. The plots of ln(σT) versus (1/T) for MAM1 film as per Mott's SPH model [34] were made and is shown in Fig. 5(a). The least square linear line was fit to the data for temperatures above θ_D, where θ_D is the Debye's temperature below which the data deviates from linearity. From the slope, the activation energy, E_a, was determined to be 12.16 meV.

For the data below θ_D, the variable-range hopping (VRH) models due to Mott [35] and Greave [36] have been applied. The plot of ln(σ) versus $T^{-1/4}$ as per Mott's (VRH) model has been made and shown in Fig.5 (b). Similarly, the plot of $\ln(\sigma T^{1/2})$ versus $T^{-1/4}$ has been sketched and shown in Fig. 5 (c). Linear lines were fit to the data at high temperatures in both the plots and density of states at Fermi level $N(E_F)$, were estimated using slopes and intercepts. The value of α required for $N(E_F)$ calculation was taken to be $10nm^{-1}$ as mentioned in reference [37,38]. The $N(E_F)$ values so obtained were $1.389X10^{28}$ $ev^{-1}cm^{-3}$ and $7.587X10^{25}$ $ev^{-1}cm^{-3}$ due to Mott's (VRH) and Greaves (VRH) models respectively. The data in the metallic region for MAM1 film was fit to the linear expression, ρ= A+BT and the coefficients of A and B were determined (Table 5).

ISSN 2347-3487

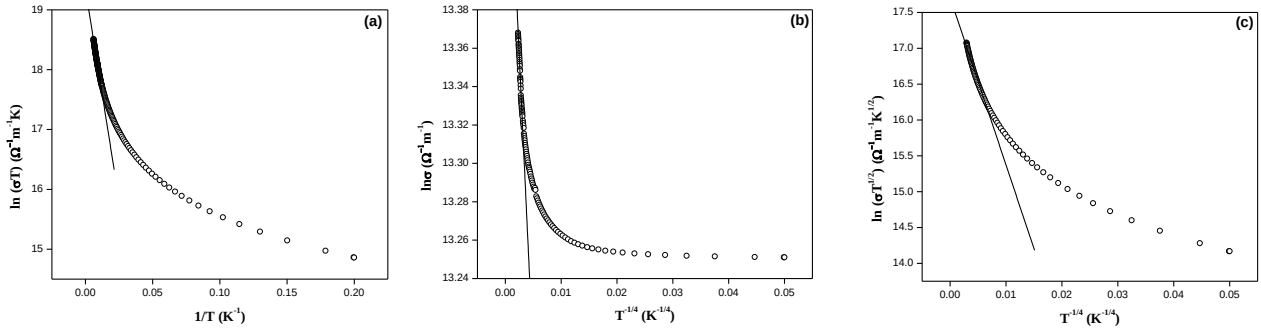

Fig. 5. The plots of (a) ln(σT) versus (1/T) for T > θ_D as per SPH model. (b) ln(σ) versus $T^{-1/4}$ for T > θ_D as per VRH model and (c) ln($\sigma T^{1/2}$) versus $T^{-1/4}$ as per Greves VRH model. Solid lines shown is the linear fit to the data.

3.4.2 Resistivity variation in MAM2 and MAM3 films

Semiconducting data of MAM2 film has been analysed using Mott's small polaron hopping model similar to that performed for MAM1. The activation energy, E_a, was determined to be 2.08 meV. Activation energies determined for MAM1 and MAM2 films are much smaller than that measured in Cu-Ni multilayers [39] and they were predicted to be due to grain boundary scattering.

The resistivity data in the semiconducting region for MAM3 was very limited and therefore, has not been considered for analysis. A careful observation of variation of ρ with T revealed that there exists three different power laws for the measured temperature range as shown in Fig.6 (a-c) for MAM3 film. Hence, the following expressions were fit to the data for different temperature ranges.

$$\rho(T) = \rho(0) + a_1 T^k \text{ for } 5K \leq T \leq 100K$$

$$\rho(T) = \rho(0) + a_2 T^m \text{ for } 45K \leq T \leq 100K$$

$$\rho(T) = A + BT^n \text{ for } 100K \leq T \leq 300K$$

Where, $\rho(0)$ is the residual resistivity which is taken to be equal to the measured value at 5K in all the films. By regressional analysis, the coefficients a_1 & a_2, exponents k, m & n and constants A & B were extracted. The fit parameters thus obtained are tabulated in Table 5. All the three films produced exponent n to be near unity. For pure nonmagnetic metals, the linearity between resistivity and temperature is expected at high temperature [40].

Table.5. The fit parameters of the MAM films.

Sample	ρ (0K) (Ωm)	ρ (300K) (Ωm)	a_1 (Ωcm K^{-k})	k	a_2 (Ωcm K^{-m})	m	A	B	n
MAM1	1.75×10^{-6}	1.54×10^{-6}	-	-	-	-	1.499×10^{-6}	1.521×10^{-10}	0.987
MAM2	1.89×10^{-6}	2.17×10^{-6}	-	-	3.179×10^{-13}	2.536	1.774×10^{-6}	1.298×10^{-9}	1.129
MAM-3	3.98×10^{-8}	1.80×10^{-7}	7.745×10^{-15}	3.4	3.511×10^{-12}	1.964	1.038×10^{-8}	5.641×10^{-10}	0.876

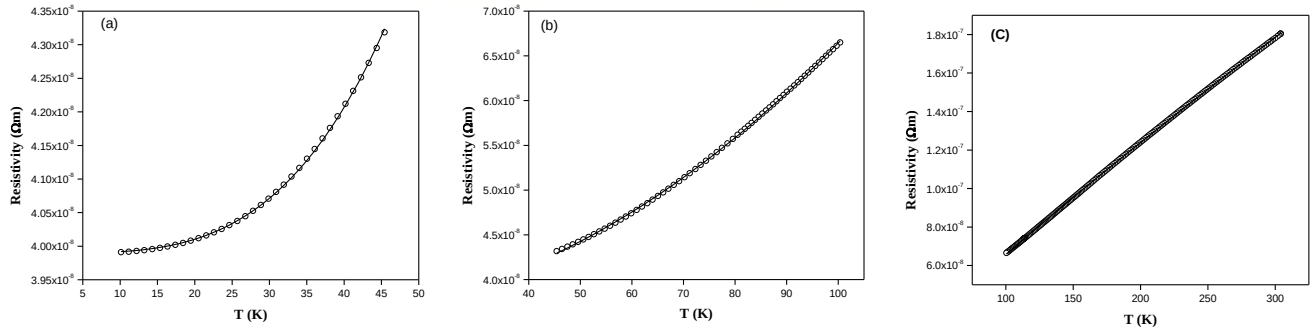

Fig.7. Plots of resistivity, ρ versus temperature, T for MAM3 film for (a) 10K to 45K (b) 45K to 100K and (c) 100K to 300K. The continuous curve passing through the data points are fits to the data.

For MAM2 and MAM3 films, in the temperature range, 45K ≤ T ≤ 100K, the exponent, m is found to be 1.96 and 2.53 respectively and that is in agreement with the results on a magnetic layer [2]. In this range of temperature, electron-phonon s-d scattering dominates over electron-magnon scattering which is expected to be dominant below 20K. For the temperature, T ≤ 45K, the exponent, k is found to be 3.34, which is greater than 2 observed for bulk Fe [41].

4. CONCLUSIONS

(i) The Multilayered films, $[Mn(60nm)/Al(20nm)]_n$; n = 1, 2 and 9 were deposited on to glass substrates by electron beam gun method at 473 K under high vacuum conditions. The structure, grain sizes, surface roughness were probed by grazing incidence X-ray diffraction (GIXRD and atomic force microscope (AFM).

(ii) At two different temperatures of 150K and 200K, magnetic hysteresis loops were recorded in a MPMS SQUID – vibrating sample magnetometer (VSM). At these two temperatures, coercive field saturation magnetization, remanent magnetization and antiferromagnetic coupling were determined and discussed.

(iii) Electrical resistivity as a function of temperature in the range from 5K to 300K has been measured by four point method for all the films. All the three films exhibited semiconducting to metal transition. The data corresponds to metallic region has been analysed and relation between resistivity and temperature were established. Semiconducting data of has been analysed polaron hopping models.

It is for the first time that antiferromagnetic interaction between Mn layers through Al layer and MST have been measured in [Mn/Al] multilayered films.

ACKNOWLEDGEMENT

Authors acknowledge the financial help received from University Grants Commission, New Delhi, India in the form of a Research Project. Also, authors acknowledge the UGC-CSR, Indore for extending experimental facilities of GIXRD, AFM, magnetic and resistivity measurements.

REFERENCE

[1] Hutchings, J.A., Newstead, V., Thomas, M.F., Sinclair, G., Joyce, E.E., and Grundy, P.J. (1999). Magnetic anisotropy in Ni/Fe and Fe/Cu/NiFe multilayers. J.Phys. Condens. Matter 11, (1999), 3449-3460.

[2] Srivastava, S. K., Ravikumar, Gupta A., Patel, R. S., Majumdar, A.K., Avasthi D. K. (2006). Swift heavy ion induced mixing in Fe/Ni multilayer. Nuclear Instruments and Methods in Physics Research, B 243, (2006) 304-312.

[3] Veres, T., Cai, M., Cochrane, R.W., Rouabhi, M., Roorda, S., and Desjardins, P. (2001). MeV Si^+ irradiation of Ni/Fe multilayers: structural, transport and magnetic properties. Thin Solid Films, 382, (2001), 172-182.

[4] Yeh, Y.C., Huang, C.W., and Lue, J.T. (2008). Electrical resistivity due to electron scattering with magnetic domain walls and magnetic properties of Ni–Fe alloy thin films. Applied Surface Science, 254, (2008), 3420-3424.

[5] Grunberg, P., (1985). Some ways to modify the spin-wave mode spectra of magnetic multilyers (invited) J. Appl. Phys. 57, (1985), 3673.

[6] Grünberg, P., Schreiber, R., Pang, Y., Brodsky, M. B., and Sowers, H., (1986). Layered Magnetic Structures: Evidence for Antiferromagnetic Coupling of Fe Layers across Cr Interlayers. Phys. Rev. Lett. 57, (1986), 2442-2445.

[7] Partha Pratim Pal and Ranjit Pati. (2008). Magnetic properties of one-dimensional Ni/Cu and Ni/Al multilayered nanowires: Role of nonmagnetic spacers. Physical Review B 77, (2008), 144430-144438.

[8] Baibich, M. N., Broto, J. M., Fert, A., Nguyen Van Dau, F., Petroff, F., Eitenne, P., Creuzet, G., Friederich, A., and Chazelas, J., (1988). Giant Magnetoresistance of (001)Fel(001)Cr Magnetic Snperlattices Phys. Rev. Lett. 61, (1988), 2472-2475.

[9] Binasch, G., Grünberg, P., Saurenbach, F., and Zinn, W., (1989). Enhanced magnetoresistance in layered magnetic structures with antiferromagnetic interlayer exchange. Phys. Rev. B 39, (1989), 4828-4830

[10] Parkin, S. S. P., More, N., and Roche, K. P., (1990). Oscillations in Exchange Coupling and Magnetoresistance in Metallic Superlattice Structures: Co/Ru, Co/Cr, and Fe/Cr. Phys. Rev. Lett. 64, (1990), 2304-2307.

[11] Kumar Dileep, Gupta Ajay. (2005). Effects of Interface Roughness on Interlayer Coupling in Fe/Cr/Fe Structure. Hyperfine Interactions. 160, (2005), 165-172.

[12] Kholin, D.I., Drovosekov, A.B., Demokritov, S.O., Rickart, M., Kreines, N.M., (2006). Noncollinear Interlayer Exchange in Fe/Cr/Fe Magnetic Structures with Different Interface Roughnesses. Phys Metals Metallography 101, (2006), S67-S69.

[13] Botana, J., Pereiro, M., Baldomir, D., Kobayashi, H., Arias, J.E. (2008). Magnetic and electronic structure of *n*Fe/3Cr/*n*Fe slabs (*n* = 1 → 6)**.** Thin Solid Films 516, (2008)**,** 5144-5149.

[14] Aliev, F.G., Moshchalkov, V.V., Bruynseraede Y., (1998). Anomalous low-temperature resistivity of metallic trilayers: Possible evidence for electron scattering on symmetrical two-level systems. Phys Rev.B 58, 7, (1998). 3625-3628.

[15] Shamsutdinov, N.R., Bottger, A.J., Tichelaar, F.D., (2006). The effect of Cu interlayers on grain size and stress in sputtered Fe–Cu multilayered thin films. Scripta Materialia. 54, (2006), 1727-1732.

[16] El Khiraouia, S., Sajieddinea, M., Hehnb, M., Robertb, S., Lenobleb, O., Bellouardb, C., Sahlaoui, M., and Benkirane, K. Magnetic studies of Fe/Cu multilayers. Physica B, 403, (2008), 2509-2514.

[17] Ding, Y. F., Chen, J. S., and Liu, E., (2005). Controlling the crystallographic orientation and easy axis of magnetic anisotropy in $L1_0$ FePt films with Cu additive. Surf. Coat. Technol. 198, (2005), 270-273.

[18] Shima, T., Takanashi, K., Takahashi, Y. K., Hono, K., Li, G. Q., and Ishio, S., (2003). High coercivity and magnetic domain observation in epitaxially grown particulate FePt thin films. J. Magn. Magn. Mater. 266, (2003), 171-177.

[19] Xu, X. H., Jin, T., Wu, H. S., Wang, F., Li, X. L., and Jiang, F. X., (2007). Nearly perfect (001)-oriented Ag/$[CoPt/C]_5$/Ag composite films deposited on glass substrates. The Solid films 515, (2007), 5471-5475.

[20] Yan Peng, Yan-ying Hu, Yao-peng Li, Hui-yuan Sun, (2007). Microstructure and Magnetic Properties of Ag/Fe/Ag Pseudo-Sandwich Nanogranular Films. Chinese Journal of Chemical Physics, Vol. 20, 6, (2007), 773.

[21] Takeuchi, T.,Hirayama, Y., and Futamoto, M., (1990). Structure and magnetic properties of Mn-Al multilayered films. Journal of Applied Physics 67, (1990), 4465

[22] Takeuchi, T., Igarashi, M., Hirayama, Y., Futamoto, M., (1995). Ferromagnetic Mn/C/Si films. J. Appl. Phys. 78, (1995), 2132.

[23] Nakatani, R., Kusano, T., Yakame, H., Yamamoto, M., (2002). Magnetic and Electric Properties in C/Mn/C/Si Multilayers. Jpn. J. Appl. Phys. 41, (2002), 5978.

[24] Nakatani, R., Yakame, H., Endo, Y., Yamamoto, M., (2003). Magnetic Properties in Mn/Si–O/Si(100)-substrate Systems and Mn/Si–O/Si Trilayers. Jpn. J. Appl. Phys. 42, (2003), 3392.

[25] Hirayama, Y., Takeuchi, T., and Futamoto, M., (1993). Layer thickness dependence of magnetic properties in Mn/Al multilayers. Journal of Applied Physics 73, (1993), 6441.

[26] Sadashivaiah, P.J., T. Sankrappa, T., Sujatha, T., et al. (2010). Structural, magnetic and electrical properties of Fe/Cu/Fe films Vacuum. 85, (2010), 466-473.

[27] Srivastava, A.K., Yu-Zhang, K., Kilian, L., Frigerio, J.M., Rivory, J., (2007). Interfacial diffusion effect on phase transitions in Al/Mn multilayered thin films. J. Mater. Sci. 42, (2007), 185-190.

[28] Sasi, B., Gopchandran, K.G., (2007). Nanostructured mesoporous nickel oxide thin films. Nanotechnology, 18, (2007), 115613.

[29] Ryoichi Nakatani, Hideo Hoshiyama, Hirotaka Yakame, Yasushi Endo, Masahiko Yamamoto., (2004). Ferromagnetism in Mn/X/Si (X = B, BN, B_4C, SiC) trilayers Science and Technology of Advanced Materials 5, (2004). 69-72.

[30] Ramanna, R., Sadashivaiah, P.J., Sankarappa, T., et al. (2014). Magnetic and Low Temperature Electrical Properties of Ni/Fe Multilayers. Electrical Engineering research, 1, 4, (2013), 96-103.

[31] Ramanna, R., Sadashivaiah, P.J., Sankarappa, T., et al. (2014). Electronic Transport at Low Temperature in Ni/Al/Ni Films. Int. Research J. of Pure & Applied Chemistry, (2014), 785-796.

[32] Ravi Kumar, Abhinav Pratap Singh, Thakur, P., Chae KH, Choi WK, Basavaraj Angadi, Kaushik, S.D., Patnaik, S., (2008). Ferromagnetism and metal-semiconducting transition in Fe-doped ZnO thin films. J. Phys D: Appl. Phys. 41, 1, (2008), 155002.

[33] Bhosle, V., Tiwari, A., Narayan, J., (2006). Metallic conductivity and metal-semiconductortransition in Ga-doped Zno. Appl. Phys. Lett. 88, (2006), 032106.

[34] Mot, N.F., (1968). Conduction in glasses containing transition metal ions. J. Non-Cryst. Solids, 1, (1968), 1-17.

[35] Mot, N.F., (1969).Conduction in non-crystalline materials. Phil. Mag. 19, (1969), 835-852.

[36] Greaves, G.N., (1973). Small polaron conduction in V_2O_5 P_2O_5 glasses. J. Non-Cryst. Solids; 11, (1973),

427-446.

[37] S.R.Elliot, Physics of amorphous materials (Longman London and New York) (1984).

[38] El-Desoky, M.M., (2003). Small polaron transport in V_2O_5-NiO-TeO_2 Glasses. J. Mater. Sci-Mater, Elect. 14, (2003), 215-221.

[39] Minenkov, A.A., Bogatyrenko, S.I., Sukhov, R.V., Kryshtal, A.P., (2014). Size Dependence of the Activation Energy of Diffusion in Multilayer Cu–Ni Films. Physics of the Solid State 56, 4, (2014), 823-826.

[40] Taylor, G.R., Isin, A., Coleman, R.E., (1968). Resistivity of Iron as a Function of Temperature and Magnetization. Phys Rev, 165, (1968), 621-631.

[41] White, G.K., Woods, S.B. (1959). Electrical and Thermal Resistivity of the Transition Elements at Low Temperatures. Philos. Trans. Royal Soc. London, 251, A.995, (1959), 273-302.